

**Application example:  
Evaluation of mechanical collisions at workplaces with collaborative robots**

Zimmermann J.<sup>1</sup>, Clermont M.<sup>1</sup>, Nischalke-Fehn G.<sup>1</sup>, Karacic N.<sup>2</sup>

1 Institute for Occupational Safety and Health of the German Social Accident Insurance (IFA), Sankt Augustin, Germany

2 BGHM (Expert Committee, German Social Accident Insurance Institution for the woodworking and metalworking industries, Mainz, Germany)

KEYWORDS: mechanical hazards; collaborative robots; safety validation; ISO 10218, ISO/TS 15066

## ABSTRACT

Over the past decade, the German Social Accident Insurance (DGUV) has supported studies in which empirical limit values for mechanical impact loads were determined. In addition, Fraunhofer IFF and the IFA have presented a methodology by which biomechanical corridors were determined for 24 body locations. The corridors can be used to define new stiffness parameters for use in measuring devices to check compliance with the empirical limit values.

With reference to an application example, we demonstrate here how the new values can be interpreted and applied in the field. Risk assessments performed at workplaces involving collaborative robots (cobots) often reveal that hands and arms are located within the danger zone. The study describes briefly how an evaluation was performed on three lightweight cobots for collaborative applications, and the results of this evaluation. In addition, the IFA has developed a tool for use with existing measuring devices, by means of which validation can be performed safely and easily. ISO/PAS 5672 supports the comparability of measurements worldwide. It also suggests how, standardization may use simple and practical solutions to assure the safety and health of workers by the use of a simplified safety diagram.

## 1 INTRODUCTION

The German Social Accident Insurance (DGUV) has funded studies in which empirical limit values for mechanical impact loads were determined (FP317, FP411, FP430). In IFA-project 5160, Fraunhofer IFF and the IFA presented a methodology for determining biomechanical corridors for 24 body locations. New stiffness parameters can be derived from the corridors and used in measuring devices to check compliance with the new empirical limit values. These stiffnesses were divided into 5 clusters (i.e. significantly fewer than set out in TS 15066) for use during measurements in the field [1]. The application example described here shows how the new values are interpreted and applied in practice.

Studies containing comparable measurements have often employed a single measuring device with only one stiffness [2]. Furthermore, comparisons performed to date make reference to the provisional limit values in TS 15066 rather than the results of recent studies [3]. Risk assessments conducted at workplaces involving collaborative robots often reveal that hands and arms are located within the danger zone. Table 1, Section 1.1 shows values for the dynamic pain pressure thresholds that serve as a reference for assessment of the hazards that arise. Table 1, Section 1.2 shows benchmarks for injury data from the literature. These data show that semi-sharp contours can already be expected to cause minor injuries at values above 0.5 (joules). Accident investigations including measurements on doors and gates show that the onset of finger fractures may also be anticipated above this limit, for example should flexion occur; Hohendorff et. al. (2012) [4] described similar observations.

**Table 1.** Section 1.1: 75th percentile of the force pain pressure threshold and stiffness values (c2) for hand and arm body locations; Section 1.2: observed benchmarks for injury data from the literature.

| Section 1.1: Pain-based limit <sup>*1 *2</sup>  |                            |                          |                       |           |                       | Body Locations   |  |  |                                 |  |  |                  |       |        |               |     |     |              |                            |                      |                     |                            |                      |                       |                            |                          |   |  |  |
|---|----------------------------|--------------------------|-----------------------|-----------|-----------------------|--|--|--|---------------------------------|--|--|------------------|-------|--------|---------------|-----|-----|--------------|----------------------------|----------------------|---------------------|----------------------------|----------------------|-----------------------|----------------------------|--------------------------|---|--|--|
| No  | Body location              | Semi-sharp               |                       | Blunt     |                       |  |  |  |                                 |  |  |                  |       |        |               |     |     |              |                            |                      |                     |                            |                      |                       |                            |                          |   |  |  |
|   |                            | Force [N]                | Stiffness (c2) [N/mm] | Force [N] | Stiffness (c2) [N/mm] |  |  |  |                                 |  |  |                  |       |        |               |     |     |              |                            |                      |                     |                            |                      |                       |                            |                          |   |  |  |
| 12  | Deltoid muscle             | 85                       | 7.1                   | 130       | 10.8                  |  |  |  |                                 |  |  |                  |       |        |               |     |     |              |                            |                      |                     |                            |                      |                       |                            |                          |   |  |  |
| 13  | Humerus                    | 115                      | 16.7                  | 160       | 23.7                  |  |  |  |                                 |  |  |                  |       |        |               |     |     |              |                            |                      |                     |                            |                      |                       |                            |                          |   |  |  |
| 14  | Radial bone                | 130                      | 18.5                  | 190       | 27.2                  |  |  |  |                                 |  |  |                  |       |        |               |     |     |              |                            |                      |                     |                            |                      |                       |                            |                          |   |  |  |
| 15  | Forearm muscle             | 130                      | 16.0                  | 170       | 20.9                  |  |  |  |                                 |  |  |                  |       |        |               |     |     |              |                            |                      |                     |                            |                      |                       |                            |                          |   |  |  |
| 16  | Arm nerve                  | 100                      | 12.0                  | 150       | 18.0                  |  |  |  |                                 |  |  |                  |       |        |               |     |     |              |                            |                      |                     |                            |                      |                       |                            |                          |   |  |  |
| 17/18   | Forefinger pad             | 235                      | 38.2                  | 410       | 66.5                  |  |  |  |                                 |  |  |                  |       |        |               |     |     |              |                            |                      |                     |                            |                      |                       |                            |                          |   |  |  |
| 19/20   | Forefinger end joint       | 175                      | 39.6                  | 400       | 89.2                  | <b>Section 1.2: Literature data for Injury</b> <table border="1"> <thead> <tr> <th colspan="3">Semi-sharp contact (FQ10 &amp; CR5)</th> </tr> <tr> <th>Benchmark values</th> <th>Force</th> <th>Energy</th> </tr> <tr> <th>Body location</th> <th>[N]</th> <th>[J]</th> </tr> </thead> <tbody> <tr> <td>(13) Humerus</td> <td>~ 185 - 230<br/>(210 - 230)</td> <td>~ 0.7 ;<br/>1.6 ; 1.1</td> </tr> <tr> <td>(15) Forearm muscle</td> <td>~ 280 - 325<br/>(295 - 390)</td> <td>~ 1.1 ;<br/>1.8 ; 1.5</td> </tr> <tr> <td>(25) Back of the hand</td> <td>~ 235 - 330<br/>(275 - 425)</td> <td>~ 0.7 ; 1.1 ;<br/>1 ; 1.4</td> </tr> <tr> <td colspan="3">~ Read from Figures in Behrens 2019 [5] approx.,<br/>( ) Behrens 2023 [6]<br/>f = female, m = male, N = Newton, J = Joule<br/>CR5=cylindrical radius of 5 mm</td> </tr> </tbody> </table> |  |  | Semi-sharp contact (FQ10 & CR5) |  |  | Benchmark values | Force | Energy | Body location | [N] | [J] | (13) Humerus | ~ 185 - 230<br>(210 - 230) | ~ 0.7 ;<br>1.6 ; 1.1 | (15) Forearm muscle | ~ 280 - 325<br>(295 - 390) | ~ 1.1 ;<br>1.8 ; 1.5 | (25) Back of the hand | ~ 235 - 330<br>(275 - 425) | ~ 0.7 ; 1.1 ;<br>1 ; 1.4 | ~ Read from Figures in Behrens 2019 [5] approx.,<br>( ) Behrens 2023 [6]<br>f = female, m = male, N = Newton, J = Joule<br>CR5=cylindrical radius of 5 mm |  |  |
| Semi-sharp contact (FQ10 & CR5)   |                            |                          |                       |           |                       |  |  |  |                                 |  |  |                  |       |        |               |     |     |              |                            |                      |                     |                            |                      |                       |                            |                          |   |  |  |
| Benchmark values  | Force                      | Energy                   |                       |           |                       |  |  |  |                                 |  |  |                  |       |        |               |     |     |              |                            |                      |                     |                            |                      |                       |                            |                          |   |  |  |
| Body location   | [N]                        | [J]                      |                       |           |                       |  |  |  |                                 |  |  |                  |       |        |               |     |     |              |                            |                      |                     |                            |                      |                       |                            |                          |   |  |  |
| (13) Humerus  | ~ 185 - 230<br>(210 - 230) | ~ 0.7 ;<br>1.6 ; 1.1     |                       |           |                       |  |  |  |                                 |  |  |                  |       |        |               |     |     |              |                            |                      |                     |                            |                      |                       |                            |                          |   |  |  |
| (15) Forearm muscle   | ~ 280 - 325<br>(295 - 390) | ~ 1.1 ;<br>1.8 ; 1.5     |                       |           |                       |  |  |  |                                 |  |  |                  |       |        |               |     |     |              |                            |                      |                     |                            |                      |                       |                            |                          |   |  |  |
| (25) Back of the hand   | ~ 235 - 330<br>(275 - 425) | ~ 0.7 ; 1.1 ;<br>1 ; 1.4 |                       |           |                       |  |  |  |                                 |  |  |                  |       |        |               |     |     |              |                            |                      |                     |                            |                      |                       |                            |                          |   |  |  |
| ~ Read from Figures in Behrens 2019 [5] approx.,<br>( ) Behrens 2023 [6]<br>f = female, m = male, N = Newton, J = Joule<br>CR5=cylindrical radius of 5 mm   |                            |                          |                       |           |                       |  |  |  |                                 |  |  |                  |       |        |               |     |     |              |                            |                      |                     |                            |                      |                       |                            |                          |   |  |  |
| 21  | Thenar eminence            | 165                      | 18.7                  | 260       | 29.5                  |  |  |  |                                 |  |  |                  |       |        |               |     |     |              |                            |                      |                     |                            |                      |                       |                            |                          |   |  |  |
| 22/23   | Palm                       | 230                      | 33.6                  | 360       | 52.0                  |  |  |  |                                 |  |  |                  |       |        |               |     |     |              |                            |                      |                     |                            |                      |                       |                            |                          |   |  |  |
| 24/25   | Back of the hand           | 135                      | 25.6                  | 250       | 48.0                  |  |  |  |                                 |  |  |                  |       |        |               |     |     |              |                            |                      |                     |                            |                      |                       |                            |                          |   |  |  |
| <sup>*1</sup> Vacuum cushion serving as a flat, firm, form-fitting thrust restraint<br><sup>*2</sup> The exclusion of bending fractures, for example in the finger region, is not permissible<br>Semi-sharp: contact body FQ10 (flat square of 14x14 mm with 2 mm radius, aluminium)<br>Blunt: contact body FZ30 (flat cylindrical end face with 30 mm diameter, made of deformable foam)<br>75th percentile of the pain pressure threshold |                            |                          |                       |           |                       |  |  |  |                                 |  |  |                  |       |        |               |     |     |              |                            |                      |                     |                            |                      |                       |                            |                          |   |  |  |

## 2 MATERIALS

Three lightweight cobots manufactured by Universal Robots were used for the tests. A UR10e, a UR5 cb3 and a UR3e were available in the laboratory. The e-series models were loaded with a payload of 50% of their rated payload. These also featured enabling switches on the control panel (3PE, Universal Robots A/S, Denmark). A probe identical to the "FQ10" contact body used in the studies on test subjects (FP317, FP411, FP430) was attached to the flange of the robot and served as the contact body.

Five CBSF series measuring devices (CoboSafe force/pressure measuring system, GTE Industrielektronik GmbH, Germany) with spring stiffnesses of 150 N/mm, 75 N/mm, 40 N/mm, 25 N/mm and 10 N/mm, in each case with a top layer with a thickness of 7 mm and a shore hardness of 70 A, were used as measuring devices. The design of these measuring devices corresponds to the measurement methodology developed by the IFA [7, 8]. The measurement data were processed in the manufacturer's CoboSafe-Vision program and logged with software support.

## 3 TEST SETUP AND PERFORMANCE

The robots under test were bolted firmly to a profiled bench top (Figure 1). The robots performed a vertical lowering movement along the z-axis. The target point was located at a distance of 50% of the robot's maximum reach in the horizontal plane in the case of the UR5 and UR10e, and approx. 300 mm from the base of the UR3e. The target point of the movement was located 1 cm above the bench top. The force value of the detection threshold was set in each robot's safety settings to the lowest possible value of 50 N (UR3e) or 100 N (UR5 and UR10e).

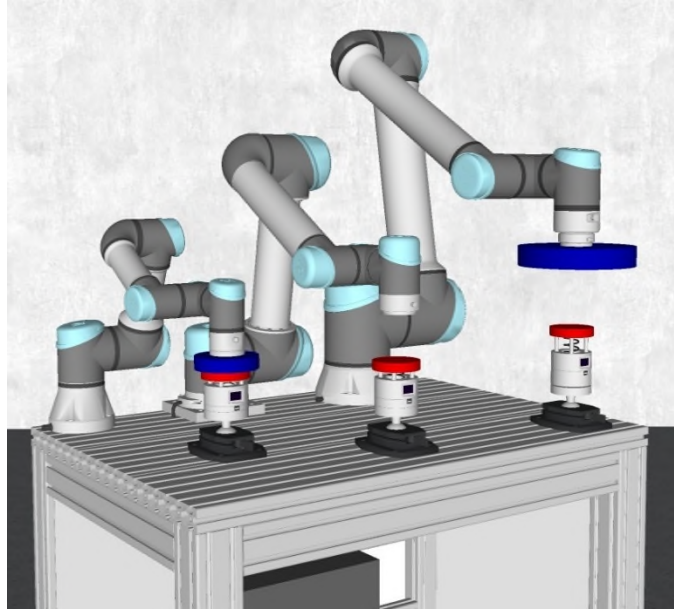


**Figure 1.** Test setup with three robot models performing a linear downward movement along the z-axis

The measuring devices were bolted firmly to the profiled plate at the target point such that the point of collision between the centre of the tool and the measuring plane was approx. 25 cm above the bench top. For design reasons, the height of the instrument varied by a few centimetres, depending upon which spring was installed. For each series of measurements, the robot's velocity was increased in increments of 50 mm/s until the maximum measuring range of the instrument in use was reached or the target velocity was no longer reached. The procedure was followed for each of the five stiffnesses and all three robot models.

#### 4 MEASUREMENT RESULTS

The measurements were used to determine objectively the hazards associated with the lowering movement described as a function of the robot velocity. Figure 2 (a) shows the results of the measurement series for a UR5 cb3. The actual stiffnesses of the measuring devices used are shown in black; the coloured lines show the robot velocities in increments of 100 mm/s. The intersections correspond to the measured forces. Energy characteristics are shown in blue for orientation purposes. The maximum force measured with a given stiffness is seen to increase with rising velocity. At low velocities, the differences between the maximum force values measured at the various stiffnesses are lower. These differences increase with rising velocity. At a given velocity, the maximum force decreases with decreasing stiffness. The energy is seen to increase at lower stiffnesses, i.e. the apparent mass of the system increases (see also [9]). A comparison between the three robot models (Figure 2 (b)) shows that at a given velocity of the tool centre point (in this case 250 mm/s), the maximum forces are lowest for the UR3e and highest for the UR10e. Owing to the increases in mass from the UR3e through the UR5 to the UR10e, this behaviour was to be anticipated.

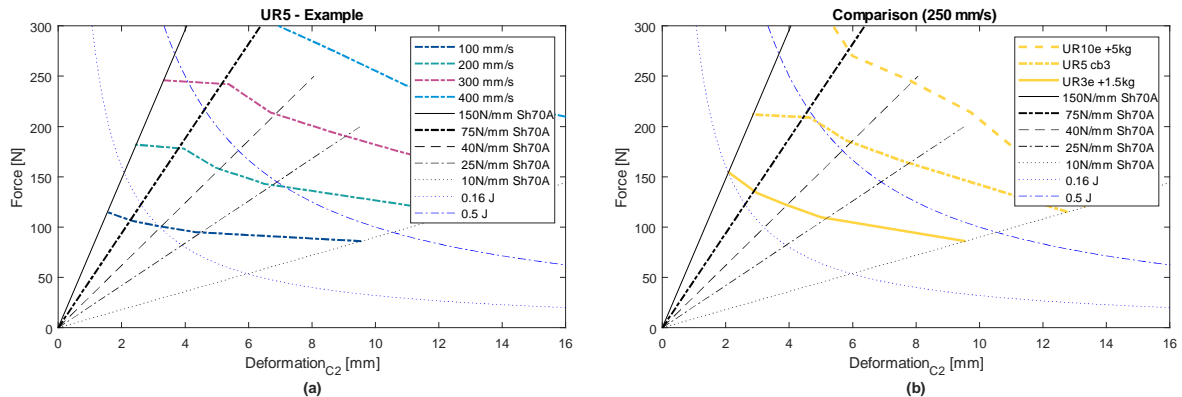


**Figure 2.** (a) Maximum forces measured at 5 stiffnesses as a function of the velocity of a UR5 cb3; (b) Comparison of the collision forces of three robot models at a velocity of 250 mm/s

## 5 COMPARISON AND EVALUATION

Besides identification of the hazards, assessment of the risk requires the stresses arising to be compared with the reference data. A safely reduced velocity can thus be identified as a measure. Figure 3 (a) shows the reference values determined for semi-sharp contact for all locations in the hand and arm body region. Figure 3 (a) shows that at the settings defined in the test and at half payload, velocities of approx. 300 mm/s may be reached with the UR3e before limit values are exceeded. In addition, benchmarks of injury onsets (IO) are shown by an asterisk to emphasize the importance of compliance with the limit values. It should be noted that locations on the palm (17/18, 21, 22/23), which have a thick epidermis (upper skin layer with callus) and substantial soft tissue, are less sensitive than the other locations on the body and may therefore be more tolerant of pain and injury. In case of a blunt contact with the UR10e, bearing a payload of 5 kg, Figure 3 (b) shows that a velocity of approx. 150 mm/s leads to rise to a borderline stress.

Once a safely reduced velocity has been determined, it must be implemented as Safely Limited Speed (SLS) in the robot's safety control system. The measure can then be checked for its effectiveness and the results documented. During operation, surveillance measurements should be carried out at regular intervals to prevent technical defects from remaining undetected, or the possibility of changes on settings made by the operating personnel being reverted.

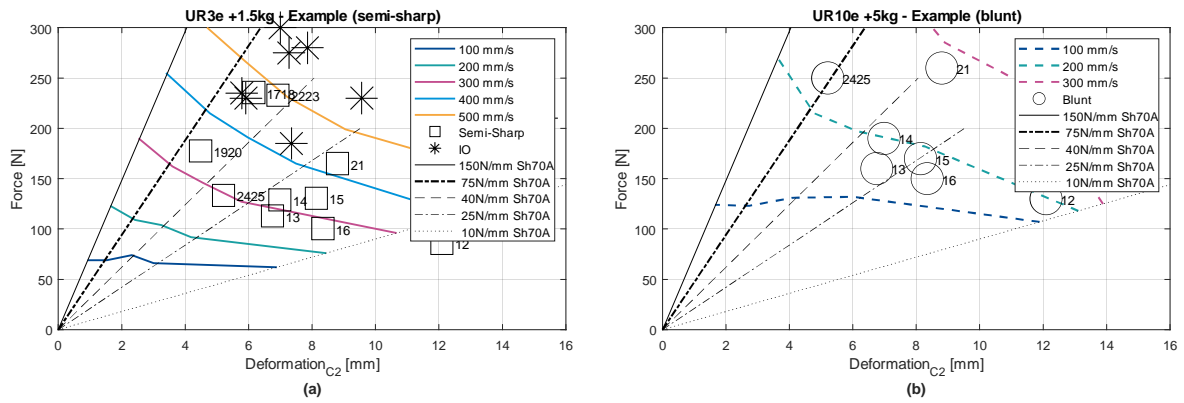


**Figure 3.** (a) Comparison of the reference data determined for semi-sharp contact with the results of measurement on a UR3e; (b): Comparison of the reference data determined for blunt contact with the results of measurement on a UR10e

## 6 LIMITS AND REQUIREMENTS

The measurement examples shown here apply only under the measurement conditions of the tests, such as the safety parameters and velocities set in the robot controller. Other payloads or changes to the lowering positions may yield different measurement results (see [10]). The most critical movement must always be evaluated. The exact stiffness of the instruments may fluctuate. The stiffnesses determined from statistical tests were assumed here. The actual stiffness may deviate slightly from these values owing to dynamic or geometric influences.

Since the contact body in this study is identical to that used in the FP317, FP411 and FP430 studies, the forces and stiffnesses from the biomechanical corridors were used here for the comparison. The base of the curve (c1, d) was ignored for the tests in this study as it lay below the detection threshold of the systems. Only the c2 stiffnesses were therefore used for this study [1, 11]. Owing to the clustering already referred to, errors of 25% occur between the stiffnesses and limit values for blunt contact. For this reason, the points do not lie exactly on the characteristic curve for the measuring device. To compensate for potential inaccuracies and losses, the limit values should be adjusted in consideration of the stiffnesses used in instruments. One such means of adjustment is for the limit values to be shifted to the actual characteristic curve of the instrument in consideration of the absorbed energy (see [12]). This approach can further reduce the number of measurements required for validation.

The recently published ISO/PAS 5672:2023 'Robotics – Collaborative applications – Test methods for measuring forces and pressures in human-robot contacts' formulates basic definitions and describes both the measuring devices and the procedure for measurement. However, it provides no guidance on how the critical test points should be determined; manufacturers, integrators, operators and standards developers are to work together in the future to develop valid statements. Critical cases may include (a) that with the lowest deformation, (b) that with the lowest maximum force/pressure and (c) that with the lowest total energy.

## 7 DISCUSSION AND FUTURE PROSPECTS

The tests show that the stresses increase with rising robot velocities. The reference data from the comparative studies enable a permissible safely reduced velocity to be determined for the application. The permissible velocities vary according to the robot model, settings, movement, payload and contact geometry. The permissible velocities in the force/power limitation are lower than those in safeguarding methods for which other safety functions are employed, such as distance monitoring.

The experience gained to date will enable a simplified measurement procedure to be developed based upon knowledge of stress limits and robot characteristics. Harmonized arrangements for this purpose should be set out in standardization activity, and procedures for measurement in the field simplified further. By judicious conversion, the number of measurements required can be further reduced. The fact that the effective or apparent mass of the system increases with decreasing stiffnesses (Figure 4 (a)) could enable measurements to be carried out solely with a soft instrument variant. This assumes that the energy generated decreases for all greater stiffnesses and that all other limit values lie above the energy characteristic.

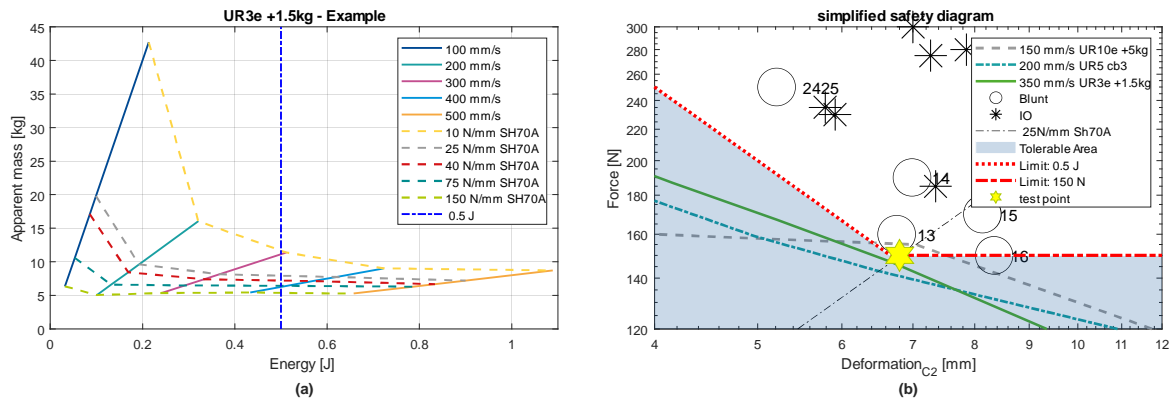


**Figure 4.** (a) Apparent mass and measured energy for different velocities and instrument stiffnesses, with reference to the example of a UR3e. (b) Simplified logarithmic safety diagram.

The available data can be used to develop a simplified safety diagram. Assuming that for a blunt geometry, a load of 150 N is acceptable and a stress of 0.5 J is tolerable, the result for this example is the limit characteristic shown in Figure 4 (b). In the diagram (logarithmic), the critical test point can be identified from the breakpoint of the curve and can be tested reasonably closely by measurement with 25 N/mm + SH70 N/mm apparatus. The figure also shows the force characteristics for the closest velocities for the three robot models. The aim is for the curves to drop off to the right below the test point down to the detection threshold.

The blunt contact body used in the studies was manufactured from elastic foam, and deformed during the tests. If a stiff contact body is used in its place, suitable minimum requirements for its geometry and dimensions must be specified for which the diagram shown is still valid. For example, flat bodies should be larger than 2 cm<sup>2</sup> and have rounded edges, cylindrical bodies should have a radius of at least 5 mm, and the radius of spherical bodies should be greater than 15 mm [6, 13 - 16]. The permissible force and the tolerable energy value may be reduced for semi-sharp contours. A pressure per unit area of 50 N/cm<sup>2</sup> can serve as a point of reference during planning; 100 N/cm<sup>2</sup> should, however, not be exceeded in practice [17, 18]. In addition, it may be necessary to set an upper limit that connects the energy line to the ordinate axis. By the formation of classes, specific requirements can be specified for manufacturers, which in turn can be used by the operator.

## 8 SUMMARY

Three robot models were used to show how biomechanical limits can be applied in the field to determine a safely reduced velocity of collaborative robots with force and power limitation. The actual velocity depends on several factors and must be determined on a case-by-case basis. The inclusion of further robot models from other manufacturers in the comparison would be desirable. This study was only one example of how the methodology can be applied. Means of attaining further simplification in the field with the aid of a safety diagram were discussed.

## 9 REFERENCES

- FP317: Experimental assessment of pain thresholds in major parts of the human body due to mechanical exposure in human-machine interface
  - FP411: Follow-up tests to the BGHM Study "Collaborative Robots: Determination of Pain Thresholds at the Human-Machine Interface"
  - FP430: Human-robot collaboration – supplementary suitability tests of recent results for incorporating them into white papers of the DGUV and standards
  - IFA-Project 5160: Development and evaluation of a metrological concept for collaborative robots
- [1] IFA-Report 2/2022: Bestimmung Biomechanischer Korridore zur Bewertung von Mechanischen Gefährdungen und Ableitung von Steifigkeitsparametern für Zukünftige Messmittel (= Determination of Biomechanical Corridors for the Evaluation of Mechanical Hazards and Estimation of Stiffness Parameters for Future Measurement Devices) (Behrens, R.; Zimmermann, J.); Deutsche Gesetzliche Unfallversicherung (DGUV): Berlin, Germany, 2022; (accessed on 9 January 2024) Available online: <https://publikationen.dguv.de/widgets/pdf/download/article/4526> (German). (English: [https://www.dguv.de/medien/ifa/en/fac/kollaborierende\\_roboter/ifa-skl\\_final\\_report.pdf](https://www.dguv.de/medien/ifa/en/fac/kollaborierende_roboter/ifa-skl_final_report.pdf))
  - [2] Scibilia, Adriano, et al. 2021 Analysis of Interlaboratory Safety Related Tests in Power and Force Limited Collaborative Robots, DOI: 10.1109/ACCESS.2021.3085109
  - [3] Behrens, R. et al: A Statistical Model to Determine Biomechanical Limits for Physically Safe Interactions With Collaborative Robots, *Front. Robot. AI*, 03.02.2022
  - [4] Hohendorff, C. Weidemann, P. Pollinger, K.J. Burkhart, M.A. Konerding, K.J. Prommersberger, P.M. Rommens: Finger injuries caused by power-operated windows of motor vehicles: an experimental cadaver study, *Injury, Int J. Care Injured* 43 (2012) 903-907
  - [5] Behrens, Roland. (2019). Biomechanische Grenzwerte für die sichere Mensch-Roboter-Kollaboration. Springer DOI: 10.1007/978-3-658-26996-8. (only in German)
  - [6] Behrens, R. et. al: A statistical model to predict the occurrence of blunt impact injuries on the human hand-arm system DOI: 10.1016/j.jbiomech.2023.111517
  - [7] M. Huelke and H. Ottersbach, "How to approve collaborating robots—The IFA force pressure measurement system," in *Proc. 7th Int. Conf. Saf. Ind. Automat. Syst. (SIAS)*, 2012, pp. 11–12.
  - [8] Zimmermann, J.; Huelke, M.; Clermont, M. Experimental Comparison of Biofidel Measuring Devices Used for the Validation of Collaborative Robotics Applications. *Int. J. Environ. Res. Public Health* 2022, 19, 13657. <https://doi.org/10.3390/ijerph192013657>
  - [9] S. Herbster, R. Behrens, N. Elkmann. (2021). A New Approach to Estimate the Apparent Mass of Collaborative Robot Manipulators. DOI: 10.1007/978-3-030-71151-1\_19.
  - [10] Schlotzhauer, L. Kaiser, J. Wachter, M. Brandstötter and M. Hofbaur, "On the trustability of the safety measures of collaborative robots: 2D Collision-force-map of a sensitive manipulator for safe HRC," 2019 IEEE 15th International Conference on Automation Science and Engineering (CASE), 2019, pp. 1676-1683, DOI: 10.1109/COASE.2019.8842991.
  - [11] Behrens, R.; Zimmermann, J.; Wang, Z.; Herbster, S.; Elkmann, N. Development of Biomechanical Response Curves for the Calibration of Biofidelic Measuring Devices Used in Robot Collision Testing. *Journal of Biomechanical Engineering* 2024, 146, 041001.
  - [12] IFA-Practical Solution: "Practical Risk Assessment Guide for Workplaces with Cobots: Conversion of Biomechanical Limit Values", Version 0.4 Beta and Application Guideline updated on 11 November 2022 <https://www.dguv.de/ifa/praxishilfen/practical-solutions-machine-safety/risikobeurteilung-von-cobots-arbeitsplaetzen-umrechnungshilfe/index.jsp> (accessed on 2 January 2024)
  - [13] Fischer C. et. al (2023): Collision Tests in Human-Robot Collaboration: Experiments on the Influence of Additional Impact Parameters on Safety DOI: 10.1109/ACCESS.2023.3327301
  - [14] Vemula B., Matthias B., Ahmad A.: A design metric for safety assessment of industrial robot design suitable for power- and force-limited collaborative operation, *International Journal of Intelligent Robotics and Applications*, 2018, DOI: 10.1007/s41315-018-0055-9
  - [15] Pungrasmi, T.; Shimaoka, Y.; Okamoto, T.; Watanabe, R. (2019): Contact Area Effects on Superficial and Deep Pain Threshold for Service Robot Safety Design using a Pain-sensing System. Development of a Human-inspired Pain-sensing System. In: *Panasonic Technical Journal* 65 (1), pp. 21-27.
  - [16] Morita, Y. and Yamada Y.: The effect of the radius of curvature of the base edge of the robot covered with cushion covering on contact pressure in human collision, *Proceedings of the 2021 IEEE International Conference on Intelligence and Safety for Robotics Nagoya, Japan, March 4-6, 2021*
  - [17] Fujikawa T. et. al. (2021): Marmarou-type Impact Tests to Investigate Criteria for Avoiding Bruises in Extremities by Human–Robot Contact, *Proceedings of the 2021 IEEE International Conference on Intelligence and Safety for Robotics Nagoya, Japan, March 4-6, 2021*
  - [18] BG/BGIA Risk Assessment Recommendations According to Machinery Directive: Design of Workplaces with Collaborative Robots, U 001/2009e October 2009 editions, revised February 2011